Comparison of the feedback linearization plus LQR controller and the PID controller for greenhouse indoor climate

Kidist Ameha Mengesha[1], Gang-Gyoo Jin[1], Yung-Deug Son[2*]

(1. *Department of Electrical Power and Control Engineering, Adama Science and Technology University, Adama 888, Ethiopia*;
2. *Department of Mechanical Facility Control Engineering, Korea University of Technology and Education, Chungnam 31253, Republic of Korea*)

Abstract: Greenhouse environmental control systems can improve the growth and quality of the plants within greenhouses by keeping a constant environment. Greenhouse climate is a multi-input multi-output system that is significantly affected by climate factors like temperature, relative humidity, and carbon dioxide levels. Due to the nonlinearity and existence of coupling among climate factors, the designed controller should provide good control performances. This study proposed both the feedback linearization plus linear quadratic regulator (LQR) controller and the proportional-integral-derivative (PID) controller for indoor air temperature and humidity control of a greenhouse system. The nonlinear greenhouse model was transformed into its equivalent linear form using input-output feedback linearization. Then, a proportional-integral type LQR controller was designed for the linear form to achieve the overall nonlinear feedback control law. In addition, the practical PID controller was designed and its gains were tuned using a genetic algorithm by considering the integral of absolute error and control deviation, and the integral of squared error and control deviation. A set of simulation works done on the nonlinear model illustrates the effectiveness of the two control methodologies. Two control methods, feedback linearization plus LQR and PID, demonstrated effective performance in both setpoint tracking and disturbance rejection. The feedback linearization plus LQR controller exhibited superior disturbance rejection capabilities, characterized by reduced perturbation peaks and faster recovery times. Conversely, the PID controller demonstrated superior setpoint tracking performance with minimal overshoot.

Keywords: greenhouse, climate control, feedback linearization plus LQR control, PID control, genetic algorithm
DOI: 10.25165/j.ijabe.20251801.8766

Citation: Mengesha K A, Jin G, Son Y. Comparison of the feedback linearization plus LQR controller and the PID controller for greenhouse indoor climate. Int J Agric & Biol Eng, 2025; 18(1): 74–82.

1 Introduction

A greenhouse is a transparent structure built to protect various vegetables, flowers, and any other plants against excessive cold or heat and provide proper growth conditions. The plant growth and quality depend significantly on greenhouse climate factors, such as air temperature, humidity, carbon dioxide, soil humidity, and so on. Even though greenhouse plants require proper control of these climate factors, the existence of non-linearity and strong coupling among these parameters make the control system difficult. Moreover, the greenhouse climate system is a multi-input multi-output (MIMO) system with both internal and external disturbances, and its mathematical model is characterized by both complexity and nonlinearity[1]. Hence, a technique that can provide optimal conditions for plants through the design of a better control system is required.

Recently, a number of studies to model and control greenhouse environment have been proposed in the literature, including model predictive control[2,3], proportional-integral-derivative (PID) control[4-7], linear quadratic regulator (LQR) control[8], feedback linearization control[9-11], sliding mode control[12,13], neural networks[14], fuzzy logic[15-17], and adaptive control[18]. Gruber et al.[2] proposed a nonlinear model predictive control method for regulating greenhouse temperature using a Volterra model. They aimed to improve the accuracy and efficiency of greenhouse climate control systems while reducing energy consumption. Bersani et al.[3] proposed a control strategy that uses a mathematical model to predict the temperature response of the greenhouse and adjusts the heating and cooling system accordingly, in order to maintain a desired temperature range. Several control methods have been proposed, but the PID controller has been widely used in different greenhouse climate control systems due to its feasibility and easy implementation. Hu et al.[5] proposed a non-linear PID controller tuning method based on a multi-objective optimization algorithm called NSGA-II to optimize the trade-off between control performance and energy consumption. Gao et al.[6] presented a PID controller based on Kalman filtering to improve the control performance of greenhouse temperature. The authors emphasized its potential for improving the sustainability of agriculture. Su et al.[7] demonstrated a self-tuning PID control algorithm based on a recursive least square method and validated its effectiveness through simulations and experiments. Essahafi et al.[8] proposed a new control strategy for greenhouse microclimate control based on an adaptive Generalized Linear Quadratic (GLQ) approach that has the ability to adapt to uncertainties and disturbances in the greenhouse environment.

Chen et al.[9] proposed an adaptive feedback linearization-based

Received date: 2023-12-31 **Accepted date:** 2024-11-25
Biographies: Kidist Ameha Mengesha, MSc, research interest: agricultural engineering, artificial intelligence, intelligent control, Email: kidistameha0@gmail.com; **Gang-Gyoo Jin**, PhD, Professor, research interest: intelligent control, fractal technique, optimization using genetic algorithm, Email: gjin30@gmail.com.
***Corresponding author: Yung-Deug Son**, PhD, Professor, research interest: electric machine drives, intelligent control and optimization using generalized predictive control algorithms. Department of Mechanical Facility Control Engineering, Korea University of Technology and Education, Chungnam 31253, Korea. Tel: +82-416408613, Email: ydson@koreatech.ac.kr.

predictive control strategy for greenhouse temperature control that combines feedback linearization and predictive control techniques. The designed system improved the accuracy and efficiency of temperature control. Chen et al.[12] presented a sliding mode control approach based on disturbance observer for a greenhouse climate system. The proposed method effectively tracks desired temperature and humidity levels, as shown in the simulations. Lammari et al.[13] proposed a new GA PI sliding mode control method for the MIMO greenhouse climate control system. The simulation result showed better results in accuracy and settling time compared to traditional methods. The research of Escamilla et al.[14] described the potential of artificial neural networks (ANNs) in greenhouse technology and smart agriculture. It presented the applications of ANNs, including climate control systems, crop yield prediction, and disease detection. Ali et al.[15] focused on the development and experimental validation of a fuzzy logic controller for an agricultural greenhouse. The controller regulates temperature and relative humidity to optimize plant growth. Chhipa et al.[16] proposed the use of fuzzy logic controllers to maintain an optimal internal climate for plant growth in a greenhouse. They highlight the benefits of fuzzy logic control over traditional methods and propose a new approach for controller tuning through hybridization with genetic algorithms. Vanegas et al.[17] presented fuzzy inference systems (FIS), which are a popular method for predicting and controlling greenhouse humidity due to their ability to handle uncertainty and non-linearity. An intelligent approach was designed to measure errors of the sensors adaptively[18]. A study was also conducted on decoupling control strategies for greenhouse environments. This approach utilizes coordinate transformation and state feedback to decouple system variables, followed by the implementation of a PID controller to simplify the overall system[19]. Although each of these methods possesses certain advantages, there remains potential for improvement via continued research efforts.

In this study, two design methods, that is, feedback linearization plus linear quadratic regulator (LQR) control and PID control are presented to keep the internal temperature and humidity of the greenhouse climate at the required values. For the former, the nonlinear greenhouse model is transformed into its equivalent linear form using input-output feedback linearization. Then, a proportional-integral type LQR controller is designed for the decoupled linear form to achieve the nonlinear feedback control law. For the latter, the practical PID controller is considered to manipulate the system outputs to reduce the derivative kick phenomenon that may occur in an ideal derivative action. The gains of the PID controller are tuned using a genetic algorithm by minimizing the integral of absolute error and control deviation (IAEU) and the integral of squared error and control deviation (ISEU). The effectiveness of the proposed methods is illustrated through a set of simulation works on the nonlinear model for the daytime summer season operation.

2 Mathematical modeling of a greenhouse system

The greenhouse, integrating various physical and biological phenomena, behaves according to nonlinear characteristics[20-22]. Two physical systems for ventilation and spraying are used to regulate internal temperature and humidity. The ventilation system circulates indoor air for cooling, and the fogger system sprays fine water droplets for cooling and humidity control. The greenhouse system is highly prone to primary external disturbances, such as intercepted solar radiation, external temperature, and external humidity, unless the glazing, shading, and other disturbance rejections are chosen properly. Figure 1 shows a greenhouse indoor climate system with three external disturbances.

The dynamic behavior of the greenhouse is based on the energy balance and mass transfer equations. The overall system differential equations are given by Nazir et al.[23] as,

$$\frac{\mathrm{d}T_{\mathrm{in}}(t)}{\mathrm{d}t}=\frac{1}{C_0}[Q_h(t)+S_i(t)-\lambda' q_{\%\mathrm{fog}}(t)]-\frac{\dot{V}_{\%}(t)}{t_v}[T_{\mathrm{in}}(t)-T_{\mathrm{out}}(t)]-\frac{UA}{C_0}[T_{\mathrm{in}}(t)-T_{\mathrm{out}}(t)] \tag{1a}$$

$$\frac{\mathrm{d}H_{\mathrm{in}}(t)}{\mathrm{d}t}=\frac{1}{V'}q_{\%\mathrm{fog}}(t)+\alpha' S_i(t)-\frac{\dot{V}_{\%}(t)}{t_v}[H_{\mathrm{in}}(t)-H_{\mathrm{out}}(t)] \tag{1b}$$

where, $T_{\mathrm{in}}(t)$ and $H_{\mathrm{in}}(t)$ are the indoor temperature (°C) and humidity ratio (g H_2O/kg of dry air), respectively; $\dot{V}_{\%}(t)$, $q_{\%\mathrm{fog}}(t)$, and $Q_h(t)$ are the percentage of the maximum ventilation rate $\dot{V}_{\max}$, the maximum water capacity $q_{\mathrm{fog,max}}$ of the fog system, and the heat (W) supplied by a heater system, respectively; $S_i(t)$ is the intercepted solar radiant energy (W), $T_{\mathrm{out}}(t)$ is ambient temperature (°C), $H_{\mathrm{out}}(t)$ is the external humidity ratio (g H_2O/kg of dry air), and UA is the heat transfer coefficient of enclosure (W/K). $\lambda'=\lambda q_{\mathrm{fog,max}}$, where, λ is the latent heat of vaporization. $\alpha'=\alpha/(\lambda VH)$, where, α is the coefficient to account for shading and leaf area index.

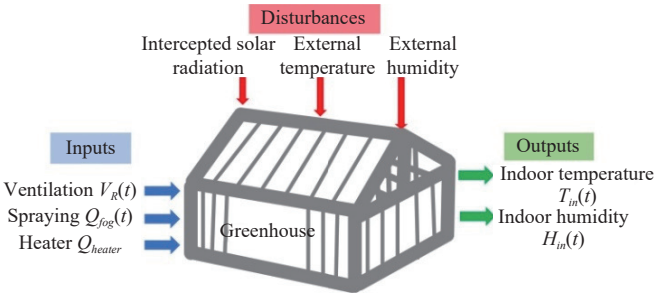

Figure 1 A greenhouse indoor climate system

The physical model of the greenhouse in Equation (1) can be used for multi-seasons, but here we consider only summer season operation. Then, the model is simplified to a two-input two-output coupled nonlinear system by setting $Q_h(t)$=0. By defining the indoor temperature $T_{\mathrm{in}}(t)$ and indoor humidity $H_{\mathrm{in}}(t)$ as state variables $x_1(t)$ and $x_2(t)$, respectively, the ventilation rate $\dot{V}(t)$ and the fog rate $q_{\mathrm{fog}}(t)$ as control variables $u_1(t)$ and $u_2(t)$, respectively, and the intercepted solar energy $S_i(t)$, the external temperature $T_{\mathrm{out}}(t)$, and the external humidity ratio $H_{\mathrm{out}}(t)$ as disturbances $d_1(t)$, $d_2(t)$, and $d_3(t)$, respectively, the following state space representation was obtained:

$$\dot{x}_1(t)=\frac{1}{C_0}[d_1(t)-\lambda' u_2(t)]-\frac{u_1(t)}{t_v}[x_1(t)-d_2(t)]-\frac{UA}{C_0}[x_1(t)-d_2(t)] \tag{2a}$$

$$\dot{x}_2(t)=\frac{1}{V'}u_2(t)+\alpha' d_1(t)-\frac{u_1(t)}{t_v}[x_2(t)-d_3(t)] \tag{2b}$$

Note that the disturbances can be measured using sensors installed in the greenhouse. Equation (2) can be rewritten in an affine form as,

$$\dot{\boldsymbol{x}}=\boldsymbol{f}(\boldsymbol{x},\boldsymbol{d})+\boldsymbol{g}(\boldsymbol{x},\boldsymbol{d})\boldsymbol{u} \tag{3a}$$

$$\boldsymbol{y}=\boldsymbol{h}(\boldsymbol{x}) \tag{3b}$$

where, $\boldsymbol{x}=[x_1\ x_2]^{\mathrm{T}}\in\Re^2$, $\boldsymbol{y}=[y_1\ y_2]^{\mathrm{T}}\in\Re^2$, $\boldsymbol{u}=[u_1\ u_2]^{\mathrm{T}}\in\Re^2$, and $\boldsymbol{d}=[d_1\ d_2\ d_3]^{\mathrm{T}}\in\Re^3$, which are the state vector, the output vector, the control input vector, and the disturbance vector, respectively. $\Re^2$ means a real vector space.

$\boldsymbol{f}$: $\Re^2 \rightarrow \Re^2$, $\boldsymbol{g}$: $\Re^{2\times 2} \rightarrow \Re^2$, and $\boldsymbol{h}$: $\Re^2 \rightarrow \Re^2$ are sufficiently smooth vector or matrix functions defined as,

$$\boldsymbol{f}(\boldsymbol{x},\boldsymbol{d}) = \begin{bmatrix} -\frac{UA}{C_0}x_1 + \frac{1}{C_0}d_1 + \frac{UA}{C_0}d_2 \\ \alpha' d_1 \end{bmatrix} \tag{3c}$$

$$\boldsymbol{g}(\boldsymbol{x},\boldsymbol{d}) = \begin{bmatrix} \boldsymbol{g}_1(\boldsymbol{x},\boldsymbol{d}) & \boldsymbol{g}_2(\boldsymbol{x},\boldsymbol{d}) \end{bmatrix} = \begin{bmatrix} \frac{1}{t_v}(d_2 - x_1) & -\frac{\lambda'}{C_0} \\ \frac{1}{t_v}(d_3 - x_2) & \frac{1}{V'} \end{bmatrix} \tag{3d}$$

$$\boldsymbol{h}(\boldsymbol{x}) = \begin{bmatrix} h_1(\boldsymbol{x}) \\ h_2(\boldsymbol{x}) \end{bmatrix} = \begin{bmatrix} x_1 \\ x_2 \end{bmatrix} \tag{3e}$$

Assuming the system operates at a steady state (u_0, x_0, and y_0), the following relationship holds:

$$\begin{aligned} \boldsymbol{u}_0 &= -\boldsymbol{g}^{-1}(\boldsymbol{x}_0,\boldsymbol{d})\boldsymbol{f}(\boldsymbol{x}_0,\boldsymbol{d}) \\ \boldsymbol{y}_0 &= \boldsymbol{h}(\boldsymbol{x}_0) \end{aligned} \tag{4}$$

3 Controller design strategies

3.1 Feedback linearization plus LQR

Feedback linearization is a powerful technique that employs nonlinear coordinate transformations to render a nonlinear system linear[10]. As can be seen from Equation (3), the outputs are indirectly related to the inputs through the state variables and the equations. Hence, it is not easy to see how the inputs can be designed to control the tracking behavior of the outputs. This difficulty can be solved by finding a direct relationship between the system outputs and the control inputs using input-output feedback linearization.

The concept of relative degree plays an important role in the analysis of nonlinear systems. This provides a necessary and sufficient condition for the existence of a full feedback linearization control law for the affine system in Equation (3). To analyze our problem further, we will employ the Lie derivative of a function h with respect to vector field f, denoted by

$$L_f h(x) = \frac{\partial h}{\partial x} f(x), \quad L_f^2 h(x) = L_f L_f h(x) = \frac{\partial (L_f h)}{\partial x} f(x),$$
$$L_f^k h(x) = L_f L_f^{k-1} h(x) = \frac{\partial (L_f^{k-1} h)}{\partial x} f(x).$$

Definition 1 (Relative degree): Consider a SISO nonlinear system as,

$$\dot{\boldsymbol{x}} = \boldsymbol{f}(\boldsymbol{x}) + \boldsymbol{g}(\boldsymbol{x})u \tag{5a}$$

$$y = h(\boldsymbol{x}) \tag{5b}$$

where, $\boldsymbol{x} \in \Re^n$, $y \in \Re$, and $u \in \Re$ are the state vector, output, and control input, respectively. $\boldsymbol{f}$: $\Re^n \rightarrow \Re^n$, $\boldsymbol{g}$: $\Re^n \rightarrow \Re^n$, and $\boldsymbol{h}$: $\Re^n \rightarrow \Re$ are sufficiently smooth vectors or functions.

Then, it is said to have a relative degree r, $1 \le r \le n$ at $\boldsymbol{x}$ in a region $D_0 \subset D$ if and only if

$$L_g L_f^i h(x) = 0 \text{ for } i = 0, 2, \ldots, r-2 \text{ but } L_g L_f^{r-1} h(\boldsymbol{x}) \neq 0 \tag{6a}$$

$$L_f h(\boldsymbol{x}) = \sum_{i=1}^{n} \frac{\partial h(\boldsymbol{x})}{\partial x_i} f_i(\boldsymbol{x}), \quad L_g h(\boldsymbol{x}) = \sum_{i=1}^{n} \frac{\partial h(\boldsymbol{x})}{\partial x_i} g_i(\boldsymbol{x}) \tag{6b}$$

To check whether feedback linearization can be applied to the system in Equation (3) or not, the relative degree of the system is examined through Theorem 1[10].

Theorem 1 (Fully feedback linearizable): Consider the MIMO nonlinear system in Equation (3). Then, the system is fully feedback linearizable, that is, the following condition is satisfied: Relative degree $r=n$, where n denotes the dimension of the system.

Proof: Finding the first derivative of the outputs in Equation (3) yields,

$$\begin{bmatrix} \dot{y}_1 \\ \dot{y}_2 \end{bmatrix} = \frac{\partial \boldsymbol{h}(\boldsymbol{x})}{\partial \boldsymbol{x}} \dot{\boldsymbol{x}} = \frac{\partial \boldsymbol{h}(\boldsymbol{x})}{\partial \boldsymbol{x}} \boldsymbol{f}(\boldsymbol{x},\boldsymbol{d}) + \frac{\partial \boldsymbol{h}(\boldsymbol{x})}{\partial \boldsymbol{x}} \boldsymbol{g}(\boldsymbol{x},\boldsymbol{d})\boldsymbol{u} = L_f \boldsymbol{h}(\boldsymbol{x}) + L_g \boldsymbol{h}(\boldsymbol{x})\boldsymbol{u} \tag{7a}$$

where,

$$L_f \boldsymbol{h}(\boldsymbol{x}) = \begin{bmatrix} L_f h_1(\boldsymbol{x}) \\ L_f h_2(\boldsymbol{x}) \end{bmatrix} \tag{7b}$$

$$L_g \boldsymbol{h}(\boldsymbol{x}) = \begin{bmatrix} L_{g_1} h_1(\boldsymbol{x}) & L_{g_2} h_1(\boldsymbol{x}) \\ L_{g_1} h_2(\boldsymbol{x}) & L_{g_2} h_2(\boldsymbol{x}) \end{bmatrix} \tag{7c}$$

Rewriting Equation (7) yields,

$$\begin{aligned} \dot{y}_1 =& L_f h_1(\boldsymbol{x}) + L_{g_1} h_1(\boldsymbol{x}) u_1 + L_{g_2} h_1(\boldsymbol{x}) u_2 = [1 \quad 0]\boldsymbol{f}(\boldsymbol{x},\boldsymbol{d}) + \\ & [1 \quad 0] \begin{bmatrix} \frac{1}{t_v}(d_2 - x_1) \\ \frac{1}{t_v}(d_3 - x_2) \end{bmatrix} u_1 + [1 \quad 0] \begin{bmatrix} -\frac{\lambda'}{C_0} \\ \frac{1}{V'} \end{bmatrix} u_2 = \\ & -\frac{UA}{C_0}x_1 + \frac{1}{C_0}d_1 + \frac{UA}{C_0}d_2 + \frac{1}{t_v}(d_2 - x_1)u_1 - \frac{\lambda'}{C_0}u_2 \end{aligned} \tag{8a}$$

$$\begin{aligned} \dot{y}_2 =& L_f h_2(\boldsymbol{x}) + L_{g_1} h_2(\boldsymbol{x}) u_1 + L_{g_2} h_2(\boldsymbol{x}) u_2 = [1 \quad 0]\boldsymbol{f}(\boldsymbol{x},\boldsymbol{d}) + \\ & [1 \quad 0] \begin{bmatrix} \frac{1}{t_v}(d_2 - x_1) \\ \frac{1}{t_v}(d_3 - x_2) \end{bmatrix} u_1 + [1 \quad 0] \begin{bmatrix} -\frac{\lambda'}{C_0} \\ \frac{1}{V'} \end{bmatrix} u_2 = \\ & \alpha' d_1 + \frac{1}{t_v}(d_3 - x_2)u_1 + \frac{1}{V'}u_2 \end{aligned} \tag{8b}$$

Since at least one of the inputs appears explicitly in the equation for the first derivative of both y_1 and y_2, it is clearly shown that the relative degree of each output is 1, that is, $r_1=r_2=1$. Hence, the total relative degree $r=r_1+r_2$ is equal to the system dimension of 2 and the full-state feedback controller design is possible.

3.2 PI-type LQR control incorporating feedback linearization

It is known by Theorem 1 that the full-state feedback controller design is possible for the MIMO system in Equation (3). From Equation (7a), if $\boldsymbol{v}= [v_1\ v_2]^{\mathrm{T}}$ is chosen as,

$$\boldsymbol{v} = L_f \boldsymbol{h}(\boldsymbol{x}) + L_g \boldsymbol{h}(\boldsymbol{x})\boldsymbol{u} \tag{9a}$$

where,

$$L_f \boldsymbol{h}(\boldsymbol{x}) = f(\boldsymbol{x},\boldsymbol{d}) \tag{9b}$$

$$L_g \boldsymbol{h}(\boldsymbol{x}) = g(\boldsymbol{x},\boldsymbol{d}) \tag{9c}$$

Note that the matrix $\boldsymbol{g}(\boldsymbol{x}, \boldsymbol{d})$ in Equation (9c) must be nonsingular for the system to be I/O linearized and decoupled. The linear input-output mapping is obtained by substituting Equation (9a) into Equation (7a) as follows:

$$\begin{bmatrix} \dot{y}_1 \\ \dot{y}_2 \end{bmatrix} = \boldsymbol{v} \tag{10}$$

Defining the state variables as $z_1= y_1$, and $z_2= y_2$ with the fact that $y_1= x_1$, and $y_2= x_2$ gives the following form:

$$\dot{\boldsymbol{z}} = \boldsymbol{A}\boldsymbol{z} + \boldsymbol{B}\boldsymbol{v} \tag{11a}$$

$$\boldsymbol{y} = \boldsymbol{C}\boldsymbol{z} \tag{11b}$$

where,

$$\boldsymbol{z}=\begin{bmatrix} z_1 \\ z_2 \end{bmatrix},\ \boldsymbol{A}=\begin{bmatrix} 0 & 0 \\ 0 & 0 \end{bmatrix},\ \boldsymbol{B}=\begin{bmatrix} 1 & 0 \\ 0 & 1 \end{bmatrix},\ \text{and}\ \boldsymbol{C}=\begin{bmatrix} 1 & 0 \\ 0 & 1 \end{bmatrix} \tag{11c}$$

In designing a greenhouse indoor climate control system, exhibiting a particular desired response of the inside air temperature and humidity is the principal issue in the presence of either setpoint or disturbance changes. State feedback controllers offer a straightforward design process, exhibit robust performance in the presence of uncertainty, and improve overall system characteristics, such as rise time, overshoot, and settling time[9]. A common challenge in state feedback control is stabilizing systems against disturbances while simultaneously tracking setpoint changes. For the output to follow the desired setpoint, new state variables are defined as,

$$q_1=\int (y_1-y_{r_1})\mathrm{d}t \tag{12a}$$

$$q_2=\int (y_2-y_{r_2})\mathrm{d}t \tag{12b}$$

where, y_{r1} is the desired setpoint for y_1 and y_{r2} for y_2. Differentiating both sides of Equation (12) and combining them with Equation (11) forms an augmented equation as,

$$\dot{\tilde{\boldsymbol{z}}}=\tilde{\boldsymbol{A}}\tilde{\boldsymbol{z}}+\tilde{\boldsymbol{B}}\boldsymbol{v}-\begin{bmatrix} \boldsymbol{0} \\ \boldsymbol{I} \end{bmatrix}\boldsymbol{y}_r \tag{13a}$$

$$\boldsymbol{y}=\tilde{\boldsymbol{C}}\tilde{\boldsymbol{z}} \tag{13b}$$

where, $\tilde{\boldsymbol{z}}=[z_1\ \ z_2\ \ q_1\ \ q_2]^{\mathrm{T}}$, $\boldsymbol{y}_r=[y_{r1}\ \ y_{r2}]^{\mathrm{T}}$,

$$\tilde{\boldsymbol{A}}=\begin{bmatrix} \boldsymbol{A} & \boldsymbol{0} \\ \boldsymbol{C} & \boldsymbol{0} \end{bmatrix}=\begin{bmatrix} 0 & 0 & 0 & 0 \\ 0 & 0 & 0 & 0 \\ 1 & 0 & 0 & 0 \\ 0 & 1 & 0 & 0 \end{bmatrix},\ \tilde{\boldsymbol{B}}=\begin{bmatrix} \boldsymbol{B} \\ \boldsymbol{0} \end{bmatrix}=\begin{bmatrix} 1 & 0 \\ 0 & 1 \\ 0 & 0 \\ 0 & 0 \end{bmatrix},$$

$$\tilde{\boldsymbol{C}}=\begin{bmatrix} \boldsymbol{C} & \boldsymbol{0} \end{bmatrix}=\begin{bmatrix} 1 & 0 & 0 & 0 \\ 0 & 1 & 0 & 0 \end{bmatrix} \tag{13c}$$

State feedback involves a linear combination of the state variables to compute a control law for the augmented system. The existence of such a control law depends upon the controllability of the pair of ($\tilde{\boldsymbol{A}}$, $\tilde{\boldsymbol{B}}$). The augmented system in Equation (13) is controllable if and only if the pair ($\boldsymbol{A}$, $\boldsymbol{B}$) of the original system in Equation (11) has the rank of n and the following condition is satisfied[24]:

$$rank\begin{bmatrix} \boldsymbol{B} & \boldsymbol{A} \\ 0 & -\boldsymbol{C} \end{bmatrix}=n+p \tag{14}$$

where, n denotes the order of the original system and p is the dimension of $\boldsymbol{y}$.

From the fact that the pair ($\boldsymbol{A}$, $\boldsymbol{B}$) in Equation (11) has the rank of 2 and in Equation (14) has the rank of 4, the pair ($\tilde{\boldsymbol{A}}$, $\tilde{\boldsymbol{B}}$) is controllable. Therefore, a PI-type state feedback control law can be synthesized. There are various methods for designing a state controller[25]. In this paper, the LQR design method is adopted. The LQR provides a procedure to compute optimal control laws by minimizing a quadratic cost function:

$$J=\frac{1}{2}\int_0^{\infty}(\tilde{\boldsymbol{x}}^{\mathrm{T}}\boldsymbol{Q}\tilde{\boldsymbol{x}}+\boldsymbol{v}^{\mathrm{T}}\boldsymbol{R}\boldsymbol{v})\mathrm{d}t \tag{15}$$

where, $\boldsymbol{Q}\in\Re^{4\times4}$ is a semi-positive definite and symmetric matrix and $\boldsymbol{R}\in\Re^{2\times2}$ is a symmetric and positive definite matrix.

The optimal feedback gain matrix $\tilde{\boldsymbol{K}}$ is given by

$$\tilde{\boldsymbol{K}}=\boldsymbol{R}^{-1}\tilde{\boldsymbol{B}}^{\mathrm{T}}\boldsymbol{P} \tag{16}$$

where, $\boldsymbol{P}\in\Re^{4\times4}$ denotes a positive definite symmetric constant matrix obtained from the solution of the Riccati differential equation.

$$\boldsymbol{A}^{\mathrm{T}}\boldsymbol{P}+\boldsymbol{P}\boldsymbol{A}-\boldsymbol{P}\boldsymbol{B}\boldsymbol{R}^{-1}\boldsymbol{B}^{\mathrm{T}}\boldsymbol{P}+\boldsymbol{Q}=\boldsymbol{0} \tag{17}$$

Proper weighting matrix selection is crucial for successful controller design. $\boldsymbol{Q}$ is used to penalize the bad performance by minimizing the system states, while $\boldsymbol{R}$ is used for penalizing the actuator's effort (fan and fog spray). The control law for both indoor air temperature and humidity is given by

$$\boldsymbol{v}=-\tilde{\boldsymbol{K}}\tilde{\boldsymbol{z}}=-\boldsymbol{K}_p\boldsymbol{x}-\boldsymbol{K}_i\boldsymbol{q} \tag{18}$$

where, $\tilde{\boldsymbol{K}}=[\boldsymbol{K}_p\ k_{i1}\ k_{i2}]$ and $\boldsymbol{q}=[q_1\ q_2]^{\mathrm{T}}$. Substituting Equation (18) into Equation (9a) gives the overall control laws as,

$$\boldsymbol{u}=\boldsymbol{g}^{-1}(\boldsymbol{x},\boldsymbol{d})[\boldsymbol{v}-\boldsymbol{f}(\boldsymbol{x},\boldsymbol{d})]=\boldsymbol{g}^{-1}(\boldsymbol{x},\boldsymbol{d})\Big[-\boldsymbol{K}_p\boldsymbol{x}+k_{i1}\int(y_{r_1}-y_1)\mathrm{d}t+k_{i2}\int(y_{r_2}-y_2)\mathrm{d}t-\boldsymbol{f}(\boldsymbol{x},\boldsymbol{d})\Big] \tag{19}$$

The block diagram of the overall control system is illustrated in Figure 2.

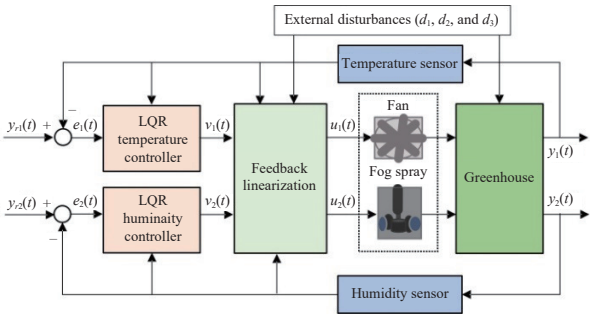

Figure 2 Closed-loop system structure with feedback linearization plus LQR control

When the large setpoint is abruptly changed, the controller output can exceed the limit values of the actuator input. Hence, input saturation is used to limit both the ventilation rate and fog rate within the range [0,1].

3.3 PID control

Due to its efficiency and easy implementation, the PID controller has been widely adopted as an alternative to greenhouse climate control[5-7]. Abrupt changes in setpoint and/or big noises may cause the derivative term of the standard PID controller to be instantaneously large, a phenomenon called *derivative kick*. Repeatedly excessive changes in input signals shorten the life of the actuator. So, in this work, the practical PID controller is used to manipulate the system outputs. Two PID controllers are expressed.

$$\frac{U_1(s)}{E_1(s)}=K_{\mathrm{pT}}+\frac{K_{\mathrm{iT}}}{s}+\frac{K_{\mathrm{dT}}s}{1+\frac{T_{\mathrm{dT}}}{N}s}\ \text{for temperature control} \tag{20}$$

$$\frac{U_2(s)}{E_2(s)}=K_{\mathrm{pH}}+\frac{K_{\mathrm{iH}}}{s}+\frac{K_{\mathrm{dH}}s}{1+\frac{T_{\mathrm{dH}}}{N}s}\ \text{for humidity control} \tag{21}$$

where, K_{pT}, K_{iT}, and K_{dT} are the proportional, integral, and derivative gains of the temperature controller, respectively. K_{pH}, K_{iH}, and K_{dH} are the proportional, integral, and derivative gains of the humidity controller, respectively. N is the derivative filter divisor, usually set to N=5-50[25], with 10 being a common choice.

Figure 3 shows the PID control system for greenhouse climate.

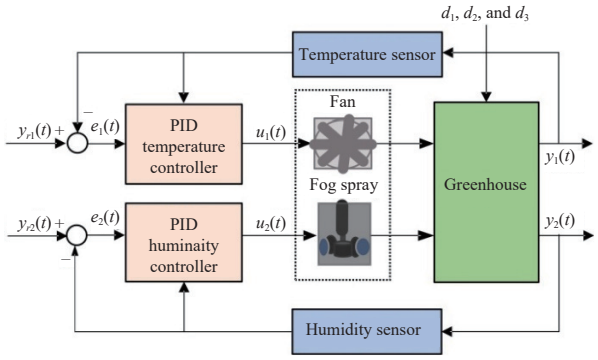

Figure 3 Closed-loop system structure with PID controllers

The tuning of controller gains can lead to substantial performance enhancements. Optimal tuning minimizes tracking errors while stabilizing the system. However, faster responses often require larger control inputs. For a trade-off between them, two performance criteria, IAEU and ISEU, are employed in this study.

$$\text{IAEU} = \int_0^{t_f} [|e_1(t)| + |e_2(t)| + w_1|\Delta u_1(t)| + w_2|\Delta u_2(t)|]\mathrm{d}t \quad (22)$$

$$\text{ISEU} = \int_0^{t_f} [e_1^2(t) + e_2^2(t) + w_1\Delta u_1^2(t) + w_2\Delta u_2^2(t)]\mathrm{d}t \quad (23)$$

where, $e_1(t)= y_{r1}(t)–y_1(t)$, $e_2(t)= y_{r2}(t)–y_2(t)$, $\Delta u_1(t)= u_1(t)– u_{10}$, and $\Delta u_2(t)= u_2(t)–u_{20}$. u_{10} and u_{20} denote the control inputs at an operating point as in Equation (4). w_1 and w_2 are user-defined weighting factors, and t_f is the upper bound of integration time. Selecting an appropriate value for the weighting factors in Equations (22) and (23) is one of the important tasks from a practical controller design perspective. Decreasing the weighting factor ensures a faster response of the closed-loop system, whereas increasing the weighting factor reduces unnecessarily excessive control effort at the expense of a slower response. Thus, the weighting factors should be chosen to obtain a good compromise between the swiftness of the closed-loop response and the control effort.

As seen in Equations (20) and (21), the two PID controllers have a total of six gains (K_{pT}, K_{iT}, K_{dT}, K_{pH}, K_{iH}, and K_{dH}). Tuning these gains to improve the performance of the feedback control system requires an optimization method[26]. For this, a GA is used. The following pseudocode illustrates the genetic algorithm process:

$t := 0$
Generate initial population $P(t)$ randomly
Evaluate the individuals in $P(t)$
while (criterion is not satisfied) do
  $t := t + 1$
  Select the individuals from $P(t–1)$ to reproduce $P(t)$
  Crossover the individuals in $P(t)$ with crossover probability
  Mutate the individuals in $P(t)$ with mutation probability
  Evaluate the individuals in $P(t)$
end while

4 Simulation results and discussion

This section presents a set of simulation works to demonstrate the effectiveness of the proposed controllers. The responses of the controllers are compared with each other and their performances are assessed on the nonlinear model in Equation (1). For simulation, the size of the greenhouse geometry is surface area=1000 m^2 and height=4 m. The parameters and their values of the greenhouse climate model at a nominal condition are listed in Table 1[4,5].

It is considered that the greenhouse has a shading screen that reduces the incident solar radiation energy by 60%. The disturbances d_1, d_2, and d_3 used in this simulation have initial values of 300 W, 35°C, and 4 g H_2O/kg, respectively. The initial values $x_1(0)$ and $x_2(0)$ of inside air temperature and internal humidity ratio are set to 30°C and 18 g H_2O/kg for the daytime of the summer season, respectively. Also, the ventilation rate and fog rates are taken in the range of 0 and 1.

Table 1 Parameter values of the greenhouse model for summer season operation

Parameters	Values with units
UA	29.81 W/°C
Co	−324.67 min·W/°C
tv	3.41 min
V'	0.0752 g/m^3·min
α'	0.0033 g/m^3·min·W
λ'	465 W

Simulations are conducted to evaluate three performance criteria: setpoint tracking, disturbance rejection, and noise reduction. The tracking performance is measured in terms of the rise time t_r, settling time t_s, overshoot M_p, integral absolute error IAE, and total variation of the control effort TV. The regulation performance is measured in terms of the peak time t_{peak}, perturbance peak M_{peak}, recovery time t_{rcy}, IAE, and TV. IAE and TV are defined as,

$$\text{IAE} = \int_0^{t_f} |e(t)|\mathrm{d}t \quad (24)$$

$$\text{TV} = \sum_{i=1}^{m-1} |u_{i+1} - u_i| \quad (25)$$

where, $e= y_{r1}–y_1$ or $y_{r2}–y_2$. u_i is the control input at the ith iteration, and m is the number of the computed inputs. M_{peak} denotes $|y_{max}–y_r|$ or $|y_{min}–y_r|$, and t_{rcy} is the time that it takes for y to recover within 2% of y_r. For our convenience, the abbreviations of "FL-LQR" for the feedback linearization plus LQR controller, "PID-IAEU" for the PID controller tuned based on the IAEU performance index, and "PID-ISEU" for the PID controller tuned based on the ISE performance index are used.

4.1 Controller settings

Although LQR provides control input in terms of minimizing the quadratic performance index in Equation (15), user-defined $\boldsymbol{Q}$ and $\boldsymbol{R}$ affect the overall performance. For this optimal control problem, the following weighting matrices were found by trial and error.

$$\boldsymbol{Q} = diag(1, 1, 15, 20) \text{ and } \boldsymbol{R} = diag(10, 10) \quad (26)$$

With this choice of $\boldsymbol{Q}$ and $\boldsymbol{R}$, the feedback gain matrices are given by

$$\boldsymbol{K}_p = \begin{bmatrix} 1.5967 & 0 \\ 0 & 1.7113 \end{bmatrix}, \ \boldsymbol{K}_i = \begin{bmatrix} 1.2247 & 0 \\ 0 & 1.4142 \end{bmatrix} \quad (27)$$

Meanwhile, the six gains of the PID controllers were tuned by the MATLAB GA function on the nonlinear model. The output responses were obtained for calculating IAEU and ISEU, while the set-point y_{r1} was changed from 30°C to 27°C and y_{r2} from 18 g H_2O/kg to 21 g H_2O/kg in combination with constant disturbances. Table 2 lists the tuned gains of the PID controllers.

4.2 Setpoint tracking test

In the setpoint tracking test, setpoints y_{r1} and y_{r2} are changed while disturbances remain constant. By considering a nominal condition, three simulation scenarios are considered to check the performance of the feedback control system:

Table 2 PID controller gains tuned by a GA

Performance index	Temperature controller			Humidity controller		
	K_{pT}	K_{iT}	K_{dT}	K_{pH}	K_{iH}	K_{dH}
IAEU	2.518	0.038	2.287	0.609	0.159	0.292
ISEU	1.294	0.027	2.461	0.864	0.001	0.307

Scenario 1: y_{r1} is decreased from 30°C to 27°C, and at the same time y_{r2} is increased from 18 g H_2O/kg to 21 g H_2O/kg;

Scenario 2: y_{r1} is decreased from 30°C to 27°C while y_{r2} remains constant at 18 g H_2O/kg;

Scenario 3: y_{r2} is increased from 18 g H_2O/kg to 21 g H_2O/kg while y_{r1} remains constant at 30°C.

As a result of Scenario 1, Figure 4 shows the responses of the indoor temperature with its corresponding control signal of the closed-loop system using the FL-LQR, PID-IAEU, and PID-ISEU controllers. It can be seen in the figure that the three methods perform satisfactorily in tracking the system to the setpoint, but FL-LQR provides a faster response with an acceptable overshoot for the setpoint change of temperature. Furthermore, the quantitative performance comparison is summarized in Table 3 and Figure 5. It can be seen that the PID-IAEU controller outperforms FL-LQR and PID-ISEU controllers in terms of overshooting M_p and settling time t_s.

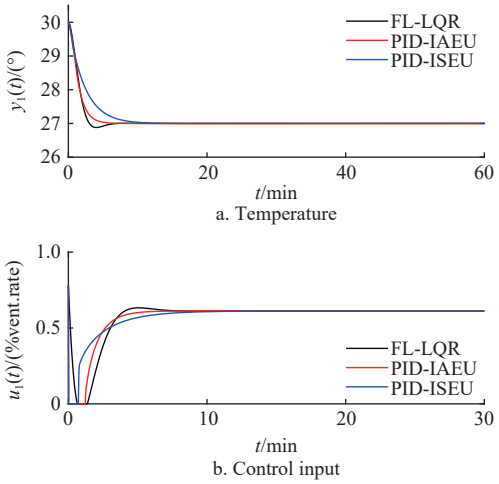

Figure 4 Responses of the three methods for stepwise setpoint changes in temperature and humidity according to Scenario 1

Table 3 Setpoint tracking performance of temperature and control input responses

Temperature controllers	Performance measures				
	M_p/%	t_r/min	t_s/min	IAE	TV
FL-LQR	4.010	1.955	5.318	4.349	1.436
PID-IAEU	0.001	2.511	4.514	4.373	1.393
PID-ISEU	0.125	4.917	8.807	7.080	1.393

Figure 6 shows the humidity responses and the control inputs conducted under the same scenario. All responses follow the setpoint well with a moderately smaller overshoot and reach the steady state within 5 min. In this simulation case, PID-ISEU shows a better response with smaller M_p and t_s as compared to the others.

Looking at Table 4 comparing the performance quantitatively, PID-IAEU shows a relatively large overshoot.

The second simulation was conducted according to Scenario 2. Figure 7 lists the responses of indoor temperature and humidity for the three controllers. Table 5 and 6 list the calculated performance.

The third simulation was conducted according to Scenario 3. Figure 8 shows the responses of indoor temperature and humidity for the three controllers. Tables 7 and 8 show the summarized performance.

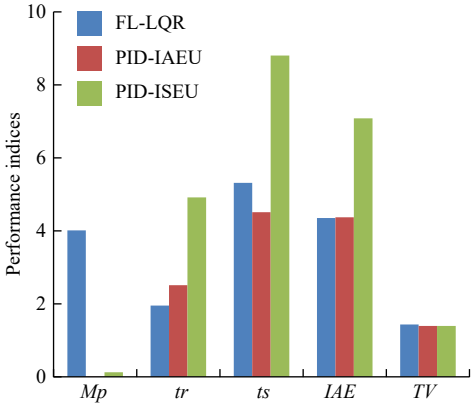

Figure 5 Performance comparison chart

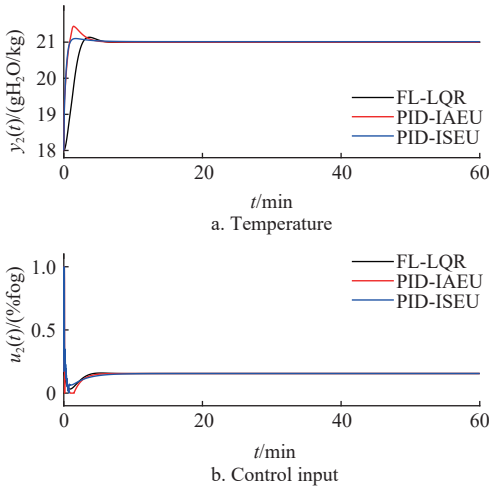

Figure 6 Responses of the three methods for stepwise setpoint changes in temperature and humidity according to Scenario 1

Table 4 Setpoint tracking performance of humidity and control input responses

Humidity controllers	Performance measures				
	M_p/%	t_r/min	t_s/min	IAE	TV
FL-LQR	4.499	1.802	4.992	4.089	1.436
PID-IAEU	14.670	0.599	4.138	1.536	1.393
PID-ISEU	3.317	0.550	3.376	1.723	1.393

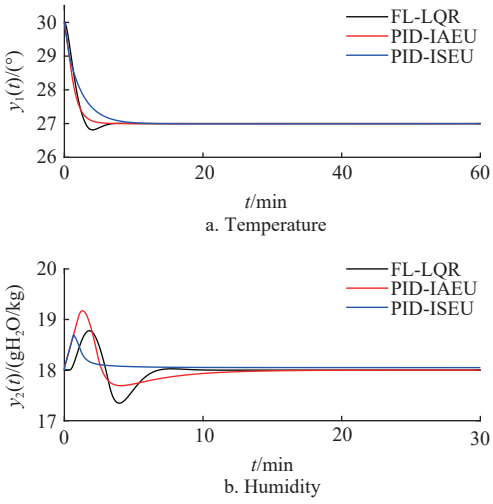

Figure 7 Responses of the three methods for stepwise setpoint changes in temperature according to Scenario 2

Table 5 Setpoint tracking performance of temperature response for Scenario 2

Temperature controllers	Performance measures				
	M_p/%	t_r/min	t_s/min	IAE	TV
FL-LQR	4.060	2.064	6.203	5.762	4.621
PID-IAEU	15.180	2.459	0.027	4.300	3.913
PID-ISEU	20.800	4.811	0.223	8.465	6.529

Table 6 Regulation performance of humidity response for Scenario 2

Humidity controllers	Performance measures			
	t_p/min	M_{peak}/(g H_2O·kg^{-1})	t_{rcy}/min	IAE
FL-LQR	1.800	0.778	8.719	2.522
PID-IAEU	1.300	1.172	13.500	3.409
PID-ISEU	0.680	0.693	>120	3.728

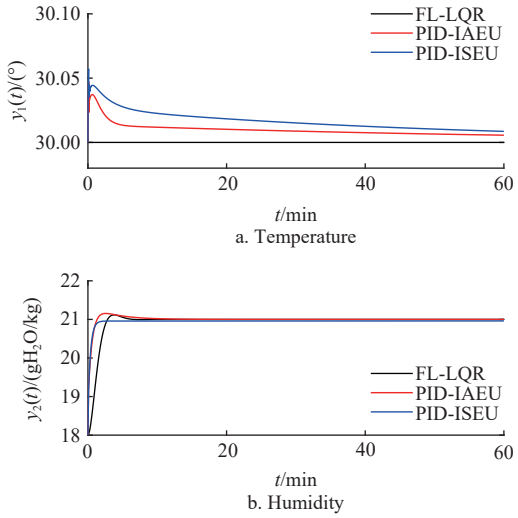

Figure 8 Responses of the three methods for stepwise setpoint changes in humidity according to Scenario 2

Table 7 Regulation performance of temperature response for Scenario 3

Temperature controllers	Performance measures			
	t_p/min	M_{peak}/°C	t_{rcy}/min	IAE
FL-LQR	0	0	0	0
PID-IAEU	0.100	0.047	>60	0.596
PID-ISEU	0.100	0.057	>60	1.019

Table 8 Setpoint tracking performance of humidity response for Scenario 3

Humidity controllers	Performance measures				
	t_p/min	M_p/%	t_r/min	t_s/min	IAE
FL-LQR	3.760	3.879	1.824	4.936	4.018
PID-IAEU	2.560	5.144	0.819	6.316	1.692
PID-ISEU	-	0	0.762	1.723	3.320

The three methods provide satisfactory responses for the setpoint change of y_{r2}, but the response y_1 of FL-LQR is maintained at the setpoint while both PID-IAEU and PID-ISEU show slow recovery to the setpoint. This can also be seen in Tables 7 and 8.

4.3 Disturbance rejection test

Although the designed controllers were optimally tuned for the purpose of setpoint tracking, the effect of disturbance affected by weather conditions was also investigated on the response of the system. The system has three disturbances, namely, intercepted solar radiant energy d_1, outside temperature d_2, and outside humidity ratio d_3. Among them, d_1 and d_2 were considered to be more variable than d_3. Step changes were introduced to the closed-loop system at 5 min, while it was operating in a steady state with y_1=27°C and y_2=21 g H_2O/kg with d_3=4 g H_2O/kg. d_1 was increased from 300 W to 500 W and d_2 was increased from 35°C to 37°C.

Figures 9 and 10 depict the responses. For FL-LQR, the closed-loop system causes a slightly larger deviation at 5 min, but it forces the output y_1 back soon toward the setpoint y_{r1}. However, PID-IAEU and PID-ISEU require more recovery time than y_{r1}. In Figure 10, the case of y_2 is similar to the previous one.

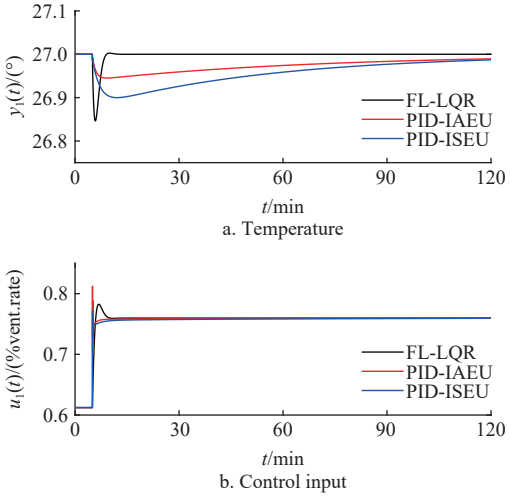

Figure 9 Responses of the three methods for stepwise disturbance changes at t=5 min

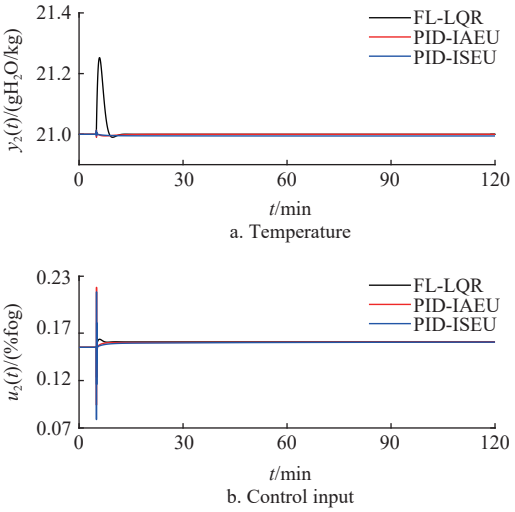

Figure 10 Responses of the three methods for stepwise disturbance changes at t=5 min

Disturbance rejection performances in terms of peak time t_{peak}, perturbance peak M_{peak}, recovery time t_{rcy}, IAE, and TV were gauged. Tables 9 and 10 list the quantitative comparison results, demonstrating FL-LQR's superior disturbance rejection performance over the PID controller.

Table 9 Quantitative comparison of the disturbance rejection performance of temperature

Temperature controllers	Performance measures				
	t_{peak}/min	M_{peak}/°C	t_{rcy}/min	IAE	TV
FL-LQR	5.840	0.154	8.799	0.299	0.194
PID-IAEU	9.160	0.056	>120	3.186	0.592
PID-ISEU	12.100	0.100	>120	5.280	0.301

Table 10 Quantitative comparison of the disturbance rejection performance of humidity

Humidity controllers	Performance measures				
	t_{peak}/min	M_{peak}/(g H_2O·kg^{-1})	t_{rcy}/min	IAE	TV
FL-LQR	5.900	0.2530	10.849	0.504	0.012
PID-IAEU	5.000	0.0132	19.613	0.036	0.468
PID-ISEU	5.000	0.0132	>120	0.611	0.501

4.4 Noise rejection test

In feedback control systems, measurement noise, which is introduced by sensors, can degrade control accuracy. To assess the effectiveness of noise attenuation strategies, a simulation study was performed. White Gaussian noise with a 20 dB signal-to-noise ratio (SNR) was superimposed on the output signal, while the setpoint was varied according to Scenario 1. Figures 11 and 12 show the output responses and the control inputs in the presence of measurement noises.

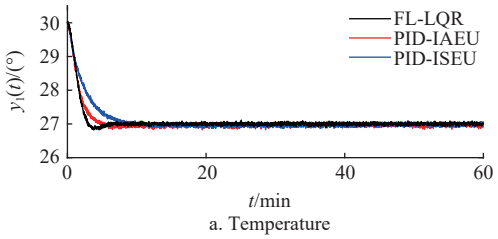

a. Temperature

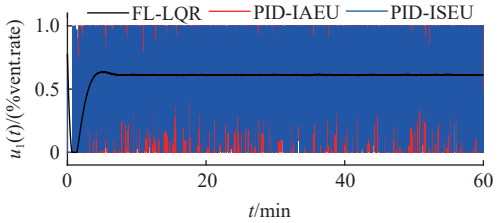

b. Control input

Figure 11 Noise rejection responses of the three methods under Gaussian noise with 20 dB SNR while the setpoints are kept constant at 28°C and 18 g H_2O/kg

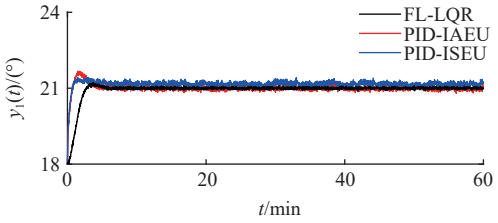

a. Temperature

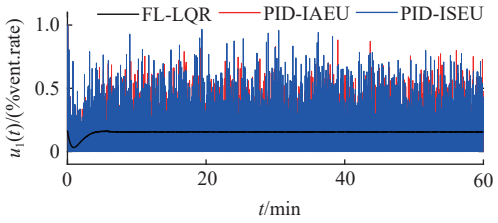

b. Control input

Figure 12 Noise rejection responses of the three methods under Gaussian noise with 20 dB SNR while the setpoints are kept constant at 28°C and 18 g H_2O/kg

Upon the stabilization of y_1 at its setpoint, y_2 likewise converges to its 21°C setpoint. Nevertheless, the PID_IAEU controller displays a slight steady-state error. Moreover, the practical PID controller suffers from derivative kick, even with the presence of a first-order filter. Figures 11 and 12 highlight the enhanced noise robustness of the FL-LQR controller.

5 Conclusions

In this study, a nonlinear greenhouse mathematical model was characterized under disturbances. The feedback linearization plus LQR controller and the PID controller for both the indoor air temperature and humidity control of a greenhouse system have been presented and their performance has been compared. The parameters of the PID controller were optimally tuned using a genetic algorithm by minimizing the performance indices, namely IAEU and ISEU. The controllers' performance was analyzed by doing both setpoint tracking and disturbance rejection tests. A set of simulation works were carried out on the nonlinear system according to designed scenarios. As expected, the two control methods showed good performances in both setpoint tracking and disturbance rejection. However, FL-LQR showed better performances in terms of disturbance rejection, with a lower perturbance peak with a short recovery time, while PID-IAEU and PID-ISEU showed good setpoint tracking performances with less overshoot.

A subsequent research endeavor is needed to implement the proposed control method in a real-world scenario and evaluate its performance.

[References]

[1] Moghaddam J J, Zarei G, Momeni D, Faridi H. Non-linear control model for use in greenhouse climate control systems. Research in Agricultural Engineering, 2022; 68: 9–17.

[2] Gruber J K, Guzman J L, Rodriguez F, Bordons C, Berenguel M. Nonlinear model predictive control of greenhouse temperature using a volterra model. In: 2009 European Control Conference (ECC), Budapest, 2009; pp.23−26. doi: 10.23919/ECC.2009.7074585.

[3] Bersani C, Ouammi A, Sacile R, Zero E. Model predictive control of smart greenhouses as the path towards near zero energy consumption. Energies, 2020; 13(14): 3647.

[4] Zeng S W, Hu H G, Xu L H, Li G H. Nonlinear adaptive PID control for greenhouse environment based on RBF network. Sensors, 2012; 12(5): 5328–5348.

[5] Hu H G, Xu L H, Goodman E D, Zeng S W. NSGA-II-based nonlinear PID controller tuning of greenhouse climate for reducing costs and improving performances. Neural Computing and Applications, 2014; 24: 927–936.

[6] Gao Z R, He L, Yue X G. Design of PID controller for greenhouse temperature based on Kalman. In: Proceedings of the 3rd International Conference on Intelligent Information Processing, 2018; pp.1−4. doi: 10.1145/3232116.3232117.

[7] Su Y P, Yu Q M, Zeng L. Parameter self-tuning PID control for greenhouse climate control problem. IEEE Access, 2020; 8: 186157–186171.

[8] Essahafi M, Lafkih M A. Microclimate control of a greenhouse by adaptive generalized linear quadratic strategy. Indonesian Journal of Electrical Engineering and Computer Science, 2018; 11: 377–385.

[9] Chen L J, Du S F, Liang M H, He Y F. Adaptive feedback linearization-based predictive control for greenhouse temperature. IFAC-PapersOnLine, 2018; 51(17): 784–789.

[10] Garces F, Becerra V M, Kambhampati C, Warwick K. Strategies for feedback linearisation. Springer, 2003; pp.27−60. doi: 10.1007/978-1-4471-0065-2.

[11] Kuo Y L, Pongpanyaporn P. Continuous-time nonlinear model predictive tracking control with input constraints using feedback linearization. Applied Sciences, 2022; 12(10): 5016.

[12] Chen L J, Du S F, Xu D, He Y F, Liang M H. Sliding mode control based on disturbance observer for greenhouse climate systems. Mathematical Problems in Engineering, 2018; 2018(1): 2071585.

[13] Lammari K, Bounaama F, Ouradj B, Draoui B. Constrained GA PI sliding mode control of indoor climate coupled MIMO greenhouse model. Journal of Thermal Engineering, 2020; 6(3): 313–326.

[14] Escamilla-Garcia A, Soto-Zarazua G M, Toledano-Ayala M, Rivas-Araiza E, Gastelum-Barrios A. Applications of artificial neural networks in greenhouse technology and overview for smart agriculture development. Applied Sciences, 2020; 10(11): 3835.

[15] Ali R B, Bouadila S, Mami A. Development of a fuzzy logic controller applied to an agricultural greenhouse experimentally validated. Applied Thermal Engineering, 2018; 141: 798–810.

[16] Chhipa I, Somwanshi D. Fuzzy logic controller to control internal climate of a greenhouse. In: 2019 4th Int. Conference and Workshops on Recent Advances and Innovations in Engineering (ICRAIE), Kedah: IEEE, 2019; pp.27−29. doi: 10.1109/ICRAIE47735.2019.9037781.

[17] Vanegas-Ayala S C, Baron-Velandia J, Leal-Lara D D. A systematic review of greenhouse humidity prediction and control models using fuzzy inference systems. Advances in Human-Computer Interaction, 2022; 2022(1): 8483003.

[18] Wang L N, Wang B R. Greenhouse microclimate environment adaptive control based on a wireless sensor network. Int J Agric & Biol Eng, 2020; 13(3): 64–69.

[19] Wu M, Xiao H, Lu C, Zhang M, Jin J, Xie X. Research on decoupling greenhouse temperature and humidity based on feedback linearization. Journal of Electrical Systems, 2024; 20(2): 394–399.

[20] Wang Y G, Lu Y J, Xiao R M. Application of nonlinear adaptive control in temperature of Chinese solar greenhouses. Electronics, 2021; 10(13): 1582.

[21] Yan H F, Acquah S J, Zhang J Y, Wang G Q, Zhang C, Darko R O. Overview of modelling techniques for greenhouse microclimate environment and evapotranspiration. Int J Agric & Biol Eng, 2021; 14(6): 1–8.

[22] Dong Q X, Liu J C, Qu M. Simple model for predicting hourly air temperatures inside Chinese solar greenhouses. Int J Agric & Biol Eng, 2023; 16(5): 56–60.

[23] Nazir T, Arslan M, Khan U S. Design of an automated greenhouse temperature controller; A renewable, robust and cost effective scheme. In: 2019 5th International Conference on Control, Automation, and Robotics (ICCAR), Beijing, 2019; pp.342−346. doi: 10.1109/ICCAR.2019.8813324.

[24] Porter B, Design of linear multivariable continuous-time tracking, International Journal of Systems Science, 2013; 5(12), 1155−1164.

[25] Levine W S. The control handbook: Control system fundamentals. Boca Raton: CRC Press, 2011; 786p.

[26] Hu H G, Xu L H, Wei R H, Zhu B K. Multi-objective control optimization for greenhouse environment using evolutionary algorithms. Sensors, 2011; 11(6): 5792–5807.